Received: 4 August 2024 | Revised: 22 October 2024 | Accepted: 6 November 2024

DOI: 10.1002/pro.5231

RESEARCH ARTICLE

THE PROTEIN SOCIETY WILEY

Controlling the *trans* effect induced by nitric oxide and carbon monoxide: H93C myoglobin versus H-NOX sensors and soluble guanylate cyclase

Byung-Kuk Yoo | **Jean-Christophe Lambry** | **Michel Negrerie**

Laboratoire d'Optique et Biosciences, INSERM U-1182, CNRS UMR 7645, Ecole Polytechnique, Palaiseau, France

Correspondence
Michel Negrerie, Laboratoire d'Optique et Biosciences, Ecole Polytechnique, 91120 Palaiseau, France.
Email: michel.negrerie@polytechnique.edu

Present address
Byung-Kuk Yoo, Thermo Fisher Scientific, Rahway, New Jersey, USA.

Review Editor: Carol Beth Post

Abstract

Myoglobin (Mb) has been engineered to replace the proximal histidine (His93) with a cysteine in order to investigate the *trans* effect induced by diatomic ligands using time-resolved electronic absorption spectroscopy. This single mutation induces a change of heme coordination state and bonding character which change carbon monoxide (CO) and nitric oxide (NO) dynamics. In H93C Mb the increased Fe^{2+}–S distance weakens this bond which is replaced with a distal Fe^{2+}–His64 ligation. We measured dynamics very different from wild type Mb but similar with those measured in soluble guanylate cyclase (sGC). Whereas NO induces a direct negative *trans* effect, the strain on His64 ligation is sufficient to counteract the positive *trans* effect due to CO. After photodissociation, geminate recombination of NO to the transient 4-coordinate heme of H93C occurred with a fast time constant (6.9 ps) identical to that in sGC. Remarkably, we also observed picosecond geminate rebinding of CO to H93C Mb, similarly with sGC in the simultaneous presence of CO and an allosteric stimulator. This CO rebinding dynamics to the 4c-heme in H93C Mb was never measured in other Mb mutants and demonstrates the existence of 5-coordinate heme with CO, explaining the synergistic activation of sGC in presence of CO and a stimulator.

KEYWORDS

carbon monoxide, guanylate cyclase, H-NOX sensors, myoglobin, nitric oxide, time-resolved absorption spectroscopy, *trans* effect

1 | INTRODUCTION

Heme sensors (Shimizu et al., 2015) from many organisms detect the diatomic ligand nitric oxide (NO) and the initial structural event after NO binding which triggers their activation varies among species and their living environment (Negrerie, 2019; Yoo et al., 2023). The activation of the mammalian NO receptor soluble guanylate cyclase (sGC) is triggered when NO induces the cleavage of the proximal His−Fe^{2+} bond in the intermediate six coordinate heme complex His−Fe^{2+}−NO (Negrerie et al., 2001; Yu et al., 1994; Zhao et al., 1999), so that the active form of sGC possesses a 5-coordinate heme with NO (5c-NO) (Dierks et al., 1997). This bond

breaking is the very first structural event which turns on the enzymatic activity of sGC for cyclic GMP synthesis from GTP. The breaking of the bond His−Fe^{2+} in sGC has been rationalized by a repulsive "*trans* effect" of NO.

The *trans* effect is a competition between the orbitals of the two opposite ligands (π* of NO and σ of histidine for d_z^2 ones) for binding to the iron (Hunt & Lehnert, 2015), leading to an increase of electron density on NO and antibonding interaction in the His−Fe^{2+} bond which becomes weaker compared to the absence of NO, as theoretically calculated (Marti et al., 2005). Structural constraints from the protein play also a fundamental role in controlling its strength (Marti et al., 2003). For example, NO induces the His−Fe^{2+} bond cleavage in α-chains, but not in β-chains of hemoglobin (Hb), clearly demonstrating the influence of the protein structure and heme environment (Petruk et al., 2013). In the H-NOX sensors family, the low energy barrier renders the cleavage of the His−Fe^{2+} bond very sensitive to temperature, but precisely modulated within same protein tertiary fold (Yoo et al., 2023).

Independently from NO, the activity of sGC can be synergistically stimulated by CO and synthetic compounds like BAY 41-2272 or its derivatives riociguat and vericiguat (Follmann et al., 2013). Time-resolved spectroscopy has allowed to demonstrate that the sGC stimulators YC-1 and BAY 41-2272 induce a conformational change of the heme environment which alters CO dynamics (Hu et al., 2008; Yoo, Lamarre, Rappaport, et al., 2012). This synergistic activation by CO and stimulators suggests that the induced protein conformational change (Kang et al., 2019) is similar to that due to NO and brings the hypothesis of counteracting the positive CO *trans* effect.

Although NO *trans* effect partially occurs in Hb (Petruk et al., 2013), it does not in myoglobin (Mb). Various studies have been performed using engineered Mb mutants, focusing on distal residues because they greatly influence the binding dynamics of diatomic ligands (Brunori et al., 1999), essentially by polarity and size of mutated distal side-chains. The proximal histidine (His93) directly bound to the heme iron also influences the binding of gas ligands to the distal side in Mb (Cao et al., 2004; Decatur et al., 1996) and its mutation is a strategy to probe structural (Hildebrand et al., 1995; Matsui et al., 1996) and catalytic properties (Adachi et al., 1991; Yoshioka et al., 2001) as well as the dynamics involved in *trans* effect (DePillis et al., 1994; Negrerie, Kruglik, et al., 2006). In particular, the mutant H93G Mb forms a mixture of 5c-NO and 6c-NO species depending on the concentration of exogenous imidazole which coordinates the heme at proximal position. Accordingly, time-resolved measurements on H93G Mb showed that geminate recombination of NO is bi-exponential due to this mixture (Negrerie, Kruglik, et al., 2006) but NO rebinding to the 4-coordinate (4c) heme was not clearly resolved as a 7-ps component as observed for truly 4c heme (Negrerie et al., 2001; Yoo et al., 2013).

Our aim was to demonstrate the existence of 5c-NO and 5c-CO species in heme proteins other than H-NOX and cytochrome c′ (AXCP). Our approach to investigate the *trans* effect induced by NO and CO binding was to introduce a constraint to the proximal heme ligand of Mb by replacing His with Cys. Cysteine is a natural internal ligand in heme-thiolate enzymes such as cytochrome P450 (Yoshioka et al., 2001) and NO-synthase, (Crane et al., 1998) and the coordination of proximal cysteine residue to heme iron has an essential enzymatic role. Likewise Gly in H93G Mb mutant, Cys can hardly interact with ferrous heme and its stabilization would require exogenous imidazole (Barrick, 1994). However, in H93C the distal histidine (His64) does bind to the heme, thus stabilized. Consequently, NO can bind to the vacant proximal side in H93C and we assumed that NO and CO dynamics in H93C would differ compared to other Mb mutants.

Here, we measured the dynamics of the heme coordination in H93C following NO or CO photodissociation on the pico- and nanosecond time scales by time-resolved absorption spectroscopy whose results were paralleled with those in sGC and wild type (WT) Mb. We measured an intrinsically fast picosecond phase (6.9 ps) of NO geminate recombination, exactly as in sGC (Yoo, Lamarre, Martin, & Negrerie, 2012) but not encountered in other Mb mutants. We also measured the geminate rebinding of CO, not observed in other Mb mutants (DePillis et al., 1994). These results support the hypothesis of counteracting the positive CO *trans* effect and the role of 5c-CO heme in the increased activity of sGC by CO in the presence of allosteric stimulators such as BAY 41-2272 (Yoo, Lamarre, Rappaport, et al., 2012).

2 | RESULTS AND DISCUSSION

2.1 | Structure of H93C and steady-state electronic absorption

We modeled the structure of H93C Mb by performing in silico mutation in the horse heart ferrous Mb structure (Protein Data Bank file 1A6G), followed by energy minimization and dynamics using CHARMM software (Brooks et al., 2009). The superposition of the structures of WT Mb and that calculated for the mutant H93C (Figure 1) indicates that this mutation does not induce any change of the whole protein tertiary fold or

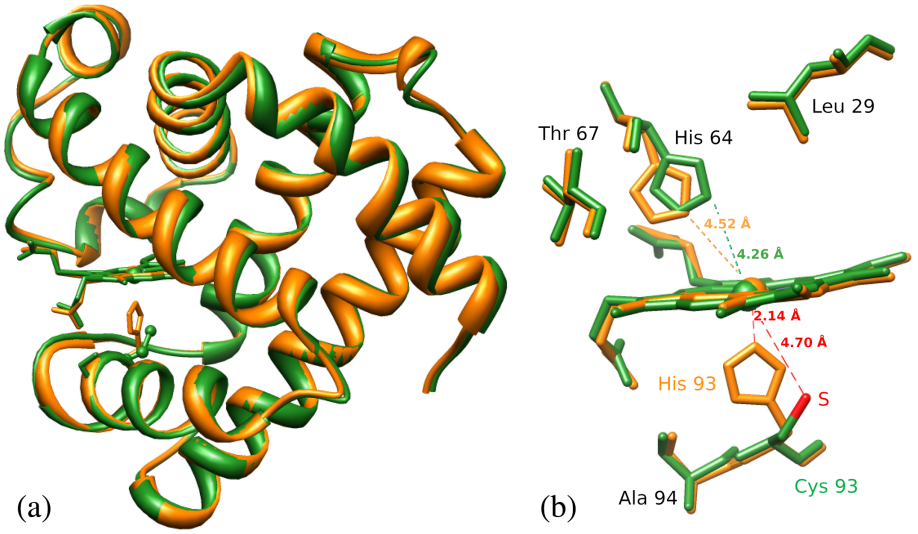

FIGURE 1 Comparison of wild type Mb and H93C Mb structures with heme in the ferrous state. (a) Superimposed tertiary structures of wild type Mb (orange) and H93C Mb (green). (b) Superposition of the ferrous heme pocket with closer side-chains. Distances are given from S atom of Cys93 to heme Fe^{2+} and from N atom of His93 and His64 to Fe^{2+} atom.

destabilization of the heme. The distance between the heme iron and His93 residue in WT Mb is 2.14 Å but the distance between the heme iron and sulfur atom of Cys93 residue is calculated to be 4.70 Å. This length is much larger than that measured for the enzyme P450 (2.2 Å) in which the heme iron is naturally linked to a thiolate (Messerschmidt et al., 2001). The structure of H93C clearly shows the vacant proximal side compared to WT Mb. The mutant structure also reveals a movement of the distal His64 toward the heme iron which also slightly moved, so that the distance decreased to 4.26 Å. These moves allow to establish an electrostatic interaction between His64 and Fe^{2+}, albeit a weak one. Other residues near the heme remain in the same coordinates after mutation.

Hilderbrand et al. showed by NMR and MCD that proximal Cys93 is coordinated to the ferric heme iron in the H93C Mb mutant, forming a 5c-Cys species (Hildebrand et al., 1995). Indeed, the position of its Soret band at 398 nm (Figure 2a) corresponds to that measured in the ferric heme-thiolate NO-synthase (Gautier et al., 2004), whereas that of the aquo-ferric heme in WT Mb would be located at 408 nm (Hoshino et al., 1996). Importantly, the coordination of the reduced heme is different. In ferrous H93C the heme is not bound to Cys93 but stabilized through electrostatic bonding of the ferrous iron with distal His64, yielding a 5c-His species (Hildebrand et al., 1995), in agreement with the Soret position at 426 nm (Figure 2a). In some way, we may consider that an inversion of distal and proximal sides occurred in the reduced form of H93C Mb. However, the terms "distal" and "proximal" sides will refer thereafter only to WT Mb for clarity.

NO can bind to both ferric and ferrous WT Mb and the H93C mutant. In H93C Mb the Soret absorption maximum appears at 400 nm after binding of NO to both ferric and ferrous hemes. This value is the same for H-NOX sensors, sGC and AXCP (Negrerie et al., 2001; Yoo et al., 2013, 2023) which form 5c-NO species, whereas in ferrous WT Mb it appears at 418 nm, characteristic of a 6c-NO species. The Q-bands also shift to that of the ferrous form (540–570 nm). We infer that the ferric heme of H93C becomes reduced and 5c-NO upon NO binding. Such reduction in the presence of NO was also observed for WT Mb (Hoshino et al., 1993, 1996). We note that it was predicted that NO adduct of the H93C mutant would be in a 5c-NO state without Cys93 coordination to the heme (Adachi et al., 1993; Hildebrand et al., 1995). Furthermore, the large distance between sulfur and Fe atoms (4.7 Å, Figure 1) creates a space for binding a diatomic in the proximal pocket. Consequently, the nitrosylated H93C is 5c-NO after the cleavage of the Fe–His64 bond induced by NO *trans* effect and must produce a 4c heme immediately after NO dissociation.

In the presence of CO the Soret maximum appears at 418 nm (Figure 2b) shifted compared to the CO complex of WT Mb which has a 6c-CO ferrous heme (Figure 2e). At this point the coordination of H93C Mb-CO is undetermined. An early study (Wayland et al., 1978) on heme models has identified the band of a heme-CO complex Soret at 419 nm (in toluene) and the Q-bands at 537 / 570 nm, matching within 1 nm the three values that we obtained in the steady-state spectrum of H93C Mb-CO. A work on sGC (Makino et al., 2018) has also identified the Soret absorption band at 417 nm as due to 5-coordinate heme-CO in the presence of a sGC activator. We thus hypothesized a 5-coordination state for H93C Mb-CO. However, there could exist an equilibrium between several species, as suggested for WT Mb at low pH (Sage et al., 1991),

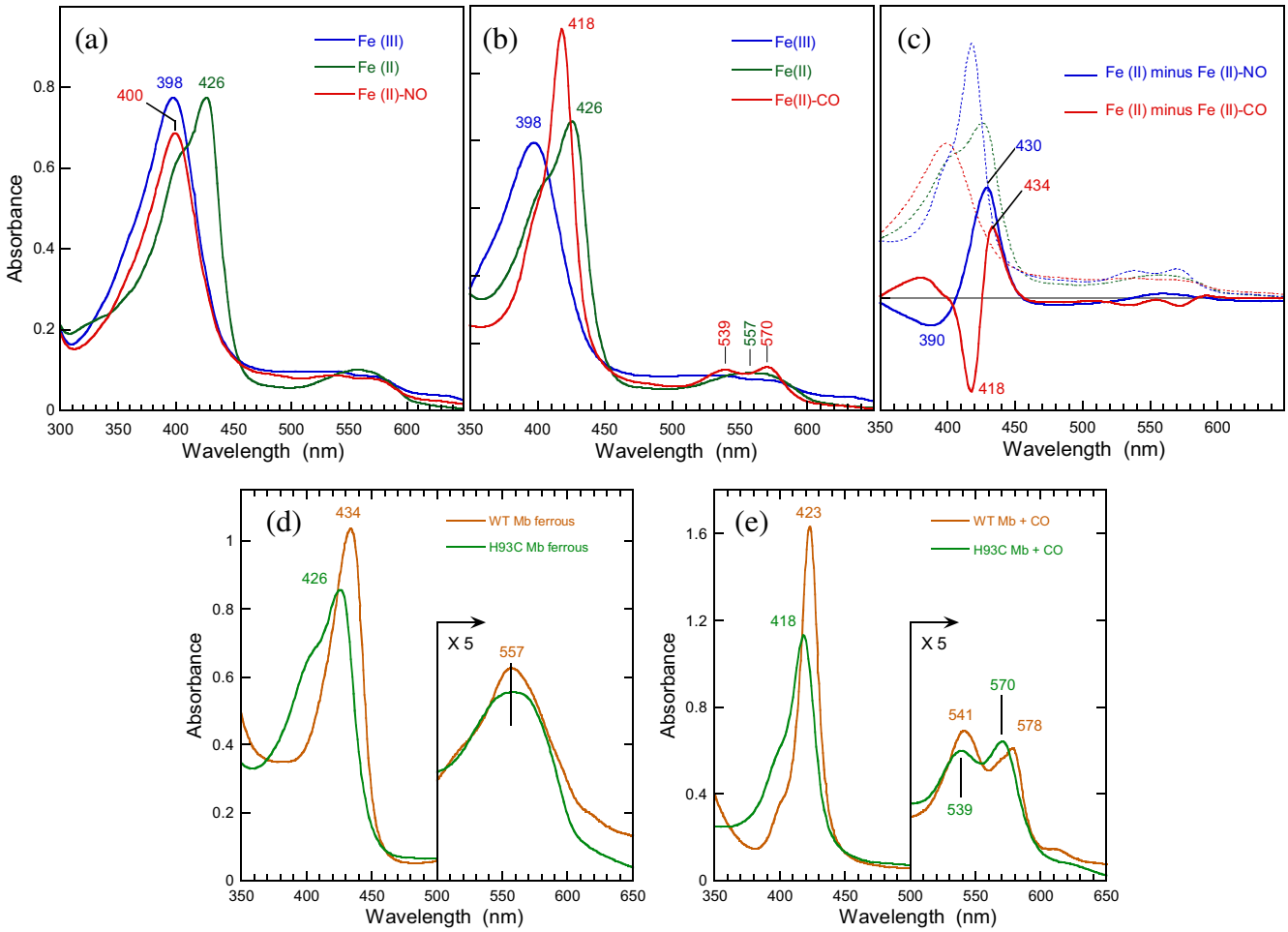

FIGURE 2 (a) Equilibrium electronic absorption spectra of ferric and ferrous H93C Mb in the absence and presence of NO. (b) in the absence and presence of CO. (c) Difference spectra for NO- and CO-bound H93C. Note the presence of a shoulder at ~398 nm (ferric 5c-Cys) in the spectrum of the unliganded ferrous species indicating that it was not fully reduced. (d) Comparison of WT and H93C Mb spectra in the unliganded ferrous state. (e) Comparison of WT and H93C Mb spectra in the CO-liganded state.

having close absorption spectra. These species can be identified by time-resolved measurements.

2.2 | Dynamics of heme and geminate rebinding of NO to H93C Mb

The initial species for time-resolved measurements is 5c-NO ferrous H93C Mb. NO is photodissociated by the excitation pulse (564 nm; ~50 fs) and transient absorption spectra at successive time delays after NO dissociation were recorded (raw data are given in Figure 3a). We first must emphasize that these transient spectra are totally different compared to those measured with endothelial NO-synthase (Negrerie et al., 1999) which has its ferrous heme coordinated with a Cys side-chain and is 6c-Cys-NO. Thus, the spectral evolution in Figure 3a does not involve Cys93 coordination. Rupture of the Fe^{2+}—NO bond from 5c-NO heme in H93C Mb induces an immediate bleaching centered at 397 nm and a broad induced absorption whose maximum is located at 429 nm. The shape of this transient spectrum (Figure 3d) is similar to that of sGC-NO (Negrerie et al., 2001; Yoo et al., 2015) and AXCP-NO (Kruglik et al., 2007) and we readily assigned the bleaching (397 nm) to the disappearance of 5c-NO heme and the induced absorption to the 4c heme. Consequently, the rapid decay of the transient spectrum within 50 ps implies the reformation of the initial species 5c-NO due to fast NO geminate rebinding to the 4c heme.

We analyzed the raw data matrix (time × wavelength) of Figure 3a by means of Singular value decomposition (SVD) to detect any contribution other than NO rebinding and we obtained spectral components (Figure 3b) whose associated kinetics describe their evolution (Figure 3e,f). The NO geminate rebinding is major and represented by the SVD1 component, but a minor spectral component SVD2 is revealed whose amplitude is

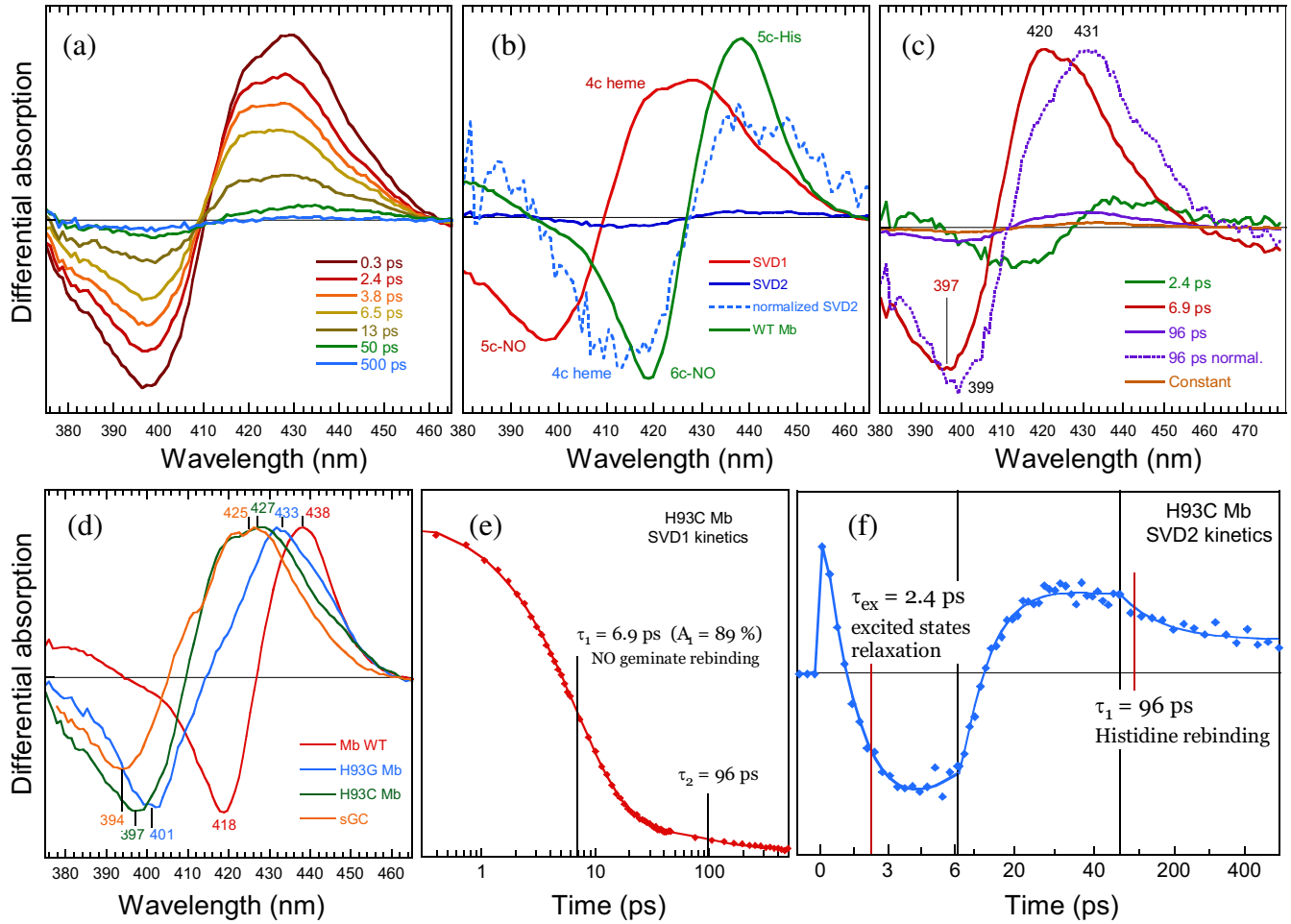

FIGURE 3 (a) Raw transient spectra at different time delays after photodissociation of NO from the ferrous heme of H93C Mb. (b) SVD spectral components obtained from the decomposition of the time–wavelength data matrix. (c) Differential absorption spectra associated with each decay components. (d) Comparison of SVD1 spectral component for four proteins: WT Mb, H93C Mb, H93G Mb and sGC. (e, f) SVD kinetic components for NO rebinding for H93C Mb up to 500 ps.

TABLE 1 Fit parameters of NO rebinding kinetics (Figure 3).

	Component SVD1					Component SVD2				
Ligand	Singular value	τ_1 (ps) (A_1)	τ_2 (ps) (A_2)	τ_3 (ps) (A_3)	Constant (A_0)	Singular value	τ_1 (ps) (A_1)	τ_2 (ps) (A_2)	τ_3 (ps) (A_3)	Constant (A_0)
NO	0.49	6.9 (0.89)	96 (0.09)	–	0.02	0.03	2.4 (0.48)	6.8 (0.44)	96 (0.05)	0.03

~16 times lower than SVD1 (ratio of singular values). Kinetics (Figure 3e,f) were fitted to a sum of exponential terms (Table 1). The SVD1 kinetic component contains two terms with time constants $\tau_1 = 6.9$ ps (89%) and $\tau_2 = 96$ ps (9%) whereas SVD2 contains the same terms (6.8 ps; 44% and 96 ps; 5%) plus a fast one (2.4 ps; 48%). The latter is assigned to the decay of heme vibrational excited states, always present when photo-exciting heme proteins (Negrerie, Cianetti, et al., 2006) and was no longer considered in the following discussion. From the amplitude of kinetic components, the spectra associated to each constant (decay-associated spectra, DAS) were calculated (Figure 3c). The DAS(6.9-ps) component represents the mono-exponential NO geminate rebinding to 4c heme, which was observed in other proteins in the 5c-NO state (Kruglik et al., 2007; Negrerie et al., 2001; Yoo

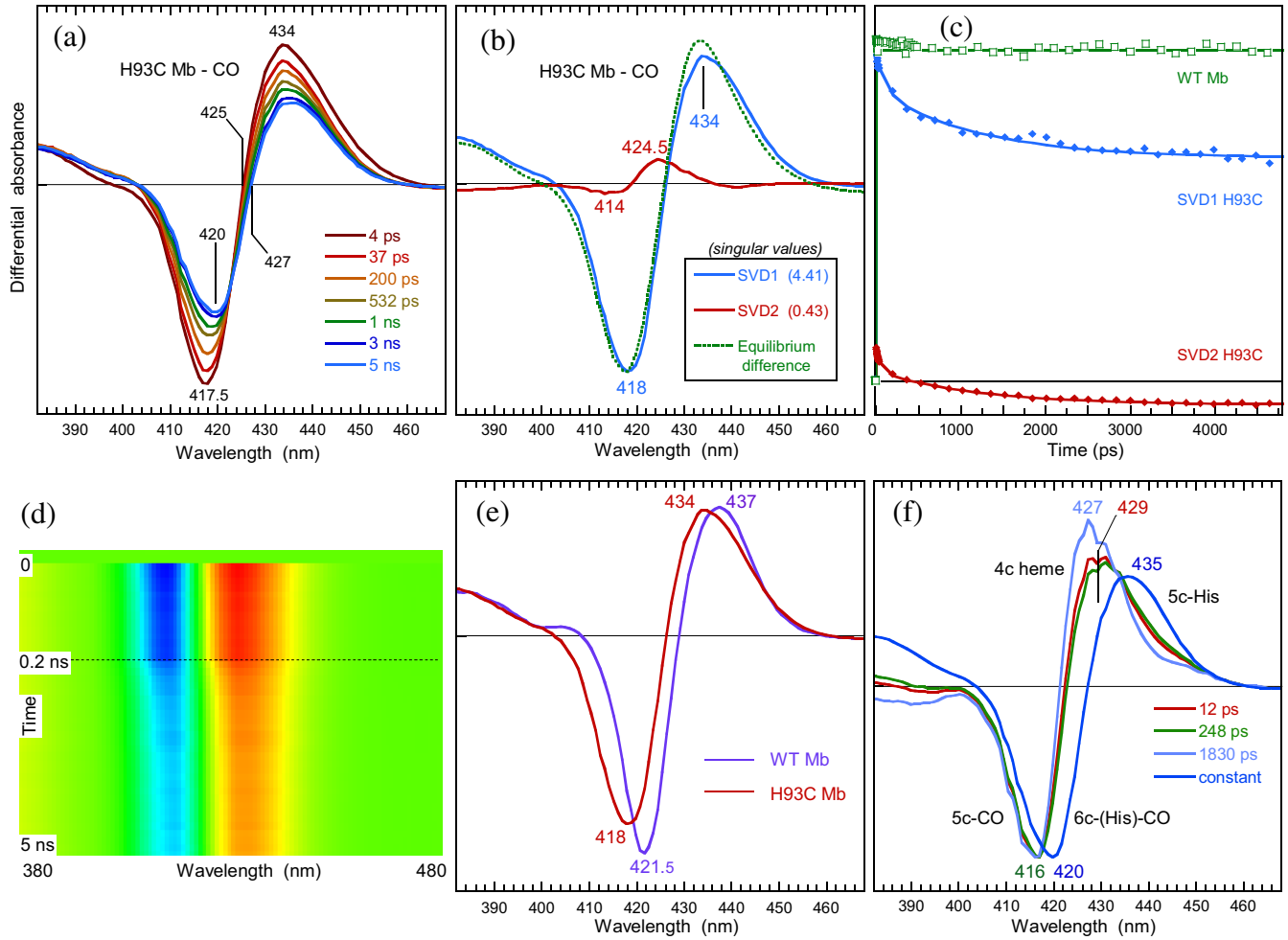

FIGURE 4 (a) Raw transient absorption spectra of H93C Mb after photodissociation of CO at different time delays up to 5 ns. (b) The two spectral components from SVD analysis compared to the equilibrium difference spectrum Mb *minus* Mb-CO. (c) Kinetic SVD components of CO rebinding to H93C up to 5 ns, compared with the unique SVD component for WT Mb. (d) Overview of the time-wavelength data matrix analyzed by global fitting. (e) Comparison of SVD1 spectral components for WT and H93C Mb. (f) Normalized differential absorption spectra, calculated from global fitting, each associated with a single time constant. They are scaled by their relative amplitudes listed in Table 2.

et al., 2023). On the other hand, the DAS(96-ps) is clearly different from the DAS(6.9-ps) and has an induced absorption band at 431 nm characteristic of a 5c-His heme, but does not correspond to 6c-NO dissociation because the bleaching is centered at 410 nm (Figure 3b), not at 419 nm like for NO rebinding to 5c-His WT Mb. The DAS(96-ps) rather corresponds to the spectrum of histidine rebinding to the 4c heme, thus assigned to this process, noting that this time constant is close to those measured for sGC (70 ps) (Yoo et al., 2015), cytochrome c′ (100 ps) (Yoo et al., 2013) and *Nostoc species* H-NOX (99 ps) (Yoo et al., 2023). The process is different from H93G Mb mutant coordinated with exogenous imidazole to replace His93 at the proximal position because free imidazole induced a mixture of species (Negrerie, Kruglik, et al., 2006).

2.3 | Dynamics of heme and geminate rebinding of CO to H93C Mb

We have previously shown that CO dynamics after photodissociation from sGC is strongly influenced by the presence of the stimulator BAY 41-2272 bound to its H-NOX heme domain (Yoo, Lamarre, Rappaport, et al., 2012). The induced conformational change potentially involves a 5c-CO species, the cleavage of the Fe^{2+}−His bond being facilitated by the presence of the stimulator. In H93C Mb the strain exerted on His64 may act similarly leading to the formation of a 5c-CO heme. We thus recorded the CO dynamics after photodissociation of the H93C−CO complex. The raw difference transient absorption spectra from 4 ps to 5 ns (Figure 4a) disclose a bleaching whose minimum experiences a shift

TABLE 2 Parameters of CO rebinding kinetics from global fitting (Figure 4).

Time constant (ps)		Amplitude A_i	Assignment
τ_1	12	0.10	4c heme → 5c-CO proximal
τ_2	248	0.15	4c heme → 5c-CO proximal
τ_3	1830	0.13	4c heme → 5c-CO distal
τ_4	Constant	0.62	5c-His64 → 6c-(His64)-CO

Note: The relative amplitudes do not include heme excited states relaxation. "Proximal" and "distal" refer to coordination in WT Mb.

from 417 to 420 nm while its amplitude decreases. The induced absorption centered at 434 nm simultaneously decays with a shift of the isosbestic point (425–427 nm). These shifts indicate that at least two processes take place, reminiscent of the CO dynamics in sGC in presence of a stimulator (Yoo, Lamarre, Rappaport, et al., 2012).

To disentangle the contributions from the different transient species, a SVD analysis of the raw data matrix was performed, yielding two distinct SVD spectral components (Figure 4b) with associated kinetic components (Figure 4c) whose ratio of singular values SV1/SV2 = 10. Both SVD spectral components clearly differ and describe different processes. We performed a global analysis of the data matrix comprising these two SVD components (Figure 4d) with the software Glotaran (Snellenburg et al., 2012), introducing the minimum number of exponential decays and we obtained an ensemble of five decay-associated spectra (DAS) each associated with a unique time constant (Figure 4f and Table 2). These spectra were never observed in WT Mb and were identified based on their profile. A spectrum decaying with 4 ps is readily assigned to vibrational excited states relaxation, as observed in all heme proteins excited in the Q-bands (Negrerie, Cianetti, et al., 2006) and will not be further discussed.

The spectrum associated with a constant amplitude must be assigned to the process 6c-(His)-CO → 5c-His because the 4c heme is very reactive (Yoo et al., 2013) and cannot produce a constant component (here $\tau > 5$ ns) and its induced absorption corresponds to the 5c-His heme. It is clearly shifted from the spectrum of the same process in WT Mb (Figure 4e), reflecting different strains exerted on the heme of both proteins.

The three DAS spectra (Figure 4f) decaying with constants $\tau_1 = 12$ ps, $\tau_2 = 248$ ps and $\tau_3 = 1.8$ ns (Table 2) due to CO geminate rebinding clearly differ from the static difference spectrum. Their induced absorption lobes are blue shifted with respect to the constant spectrum which is due to 5c-His heme. This blue shifted induced absorption is assigned to the 4c heme (Kruglik et al., 2007; Yoo et al., 2015) and therefore these three DAS are assigned to the process 4c → 5c-CO. The 12-ps spectrum, observed neither in Mb nor in other proteins, is due to fast CO recombination to the 4c heme whose iron atom is positioned within its plane, a favorable conformation for interaction of CO and Fe^{2+} orbitals (Franzen, 2002; Ionascu et al., 2005). Indeed, CO does not possess an unpaired electron contrarily to NO and the interaction of CO bonding electrons with the d_z^2 orbital of iron depends upon its position in the heme plane, creating an enthalpic barrier (Ionascu et al., 2005). Thus, the in-plane position of the iron explains the picosecond geminate recombination of CO to the 4c heme. This rebinding occurs as fast as that of NO and CO rebinds to the same heme side from which is was photodissociated, namely the proximal side where resides Cys93. The 248-ps time constant has the same spectrum as the 12-ps one and is also assigned to CO proximal rebinding to the 4c heme, but from a more distant location, noting that CO does not escape from the heme pocket on the picosecond time scale after photodissociation (Schotte et al., 2003).

Based on the spectral profile, the 1.83-ns time constant is also assigned to the 4c → 5c-CO rebinding process, but it may rather occur on the distal side because the DAS spectrum discloses a different absorption positive lobe than the 12-ps DAS, yet blue-shifted with respect to the constant spectrum so that it cannot be due to the 5c-His64 heme. This assignment agrees with the fact that the distal side is easily accessible in WT Mb and unbound CO can be present as well in both sides of heme pocket at the concentration of 1 mM in solution as employed here. The possible His rebinding (Yoo et al., 2013) cannot be detected because its relative amplitude is very minor and its DAS spectrum should be close to others. The ps components render the overall rebinding of CO to H93C much faster compared to WT Mb. All assignments are summarized in Table 2 and Scheme 1.

The 5c-CO species reformation, characterized by the bleaching at 416 nm (Figure 4f), represents 38% of the amplitude. Its identification necessitated a global analysis because it is only shifted by 4 nm from that of 6c-(His)-CO, rendering difficult to disentangle both species otherwise (whereas the 5c-NO species absorption band is largely shifted from 6c-NO by ~20 nm). In

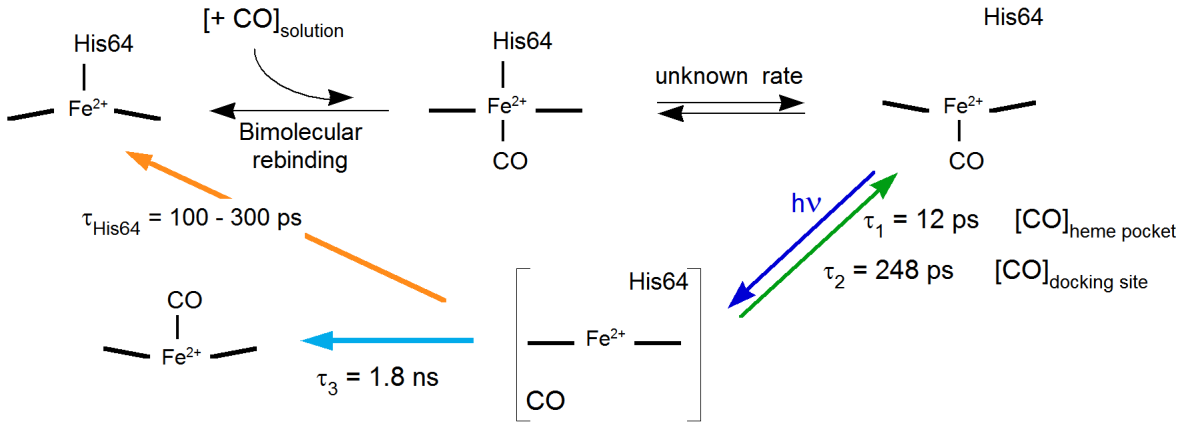

SCHEME 1 Summary of the coordination changes in H93C Mb following photodissociation of CO, which is represented by "*hν*." The rate of His64 dissociation induced by CO binding is unknown but should be in the μs to ms time range.

steady-state, the spectral shift of the Soret band between WT and H93C Mb-CO is 5 nm (418 nm vs. 423 nm, Figure 2e). The assignment of the 5c-CO species is also supported by previous studies which identified the Soret absorption band of a 5-CO porphyrin model at 419 nm (Wayland et al., 1978) and of 5-CO sGC at 417 nm (Makino et al., 2018).

The *trans* effect on the axial proximal ligand due to CO is positive and does not weaken the Fe^{2+}–His bond as shown with porphyrin models (Gullotti et al., 2007), contrary to NO which provides a negative *trans* effect (Traylor & Sharma, 1992). However, the isolated porphyrin models are devoid of protein environment which exerts constraints. The inserted heme macrocycle experiences strains as well as the proximal His ligand does, due to the protein structure, at the origin of its function modulation. The weakening of the Fe^{2+}–His bond upon CO binding was observed (Ibrahim et al., 2006), decreasing the positive *trans* effect of CO which can be canceled by proximal constraints in sGC in the presence of CO and an allosteric activator (Makino et al., 2018) leading to the partial formation of a 5-coordinate Fe^{2+}–CO species in sGC, as supported by Raman studies (Li et al., 2005; Martin et al., 2005). In brief, the positive *trans* effect of CO in heme models is not contradictory with strains which counteract it in proteins so that the Fe^{2+}–His bond can break upon CO binding as observed here for the mutated H93C Mb.

To evaluate the possibility of CO rebinding from both sides of heme pocket, we performed calculations of CO dynamics once dissociated. A CO molecule was placed in either side of the 4c heme and let free to move (see Section 3) only sterically constrained by the protein side-chains. It appears that the C atom of CO stayed within a distance (~3.6 Å) favorable for its interaction with Fe^{2+} in the proximal (Cys93) side for up to 500 ps in three calculated dynamics (Figure 5), in agreement with the two fast rebinding time constants (12 and 248 ps). In the distal (His64) side, CO stayed at ~4.8 Å in two trajectories during ~300 ps and is then positioned at 8.3 Å at 500 ps. For another trajectory CO moved farther after 150 ps, up to ~33 Å, a position which is associated with a larger time constant for rebinding, such that we have measured (1.8 ns). We remind that the distal side (His64) is the natural one for diatomics binding from solvent to the heme in WT Mb. Although not intended for deriving any statistics, these calculations fully agree with our spectroscopic measurements and assignments.

2.4 | Implications for soluble guanylate cyclase and heme sensors

Overall, our results show that the Fe^{2+}–His bond can be broken due to CO binding in certain proteins and demonstrate the existence of the 5c-CO ferrous heme. Here, a constraint was created by removing the WT proximal His93, forcing the distal H64 to bind to the heme iron. We notice that the ultrafast kinetic component of CO geminate recombination ($\tau \leq 12$ ps) is present only in H-NOX sensors prone to form a 5c-CO ferrous heme and a 4c photodissociated heme (Table 3). Such ultrafast CO rebinding component ($\tau \leq 12$ ps) is even not present in sensors with an extremely small k_{off} (3.7×10^{-6} s^{-1}) such as the L16A AXCP mutant (Andrew et al., 2016) and is not determinant for the affinity but rather for the mechanism. Its behavior with NO is the same: even having the smallest K_D ever measured among NO-sensors (6.9×10^{-14} M) due to low k_{off} (2×10^{-7} s^{-1}) the L16A AXCP mutant does not form a 5c-NO but only a 6c-(His)-NO species (Andrew et al., 2016).

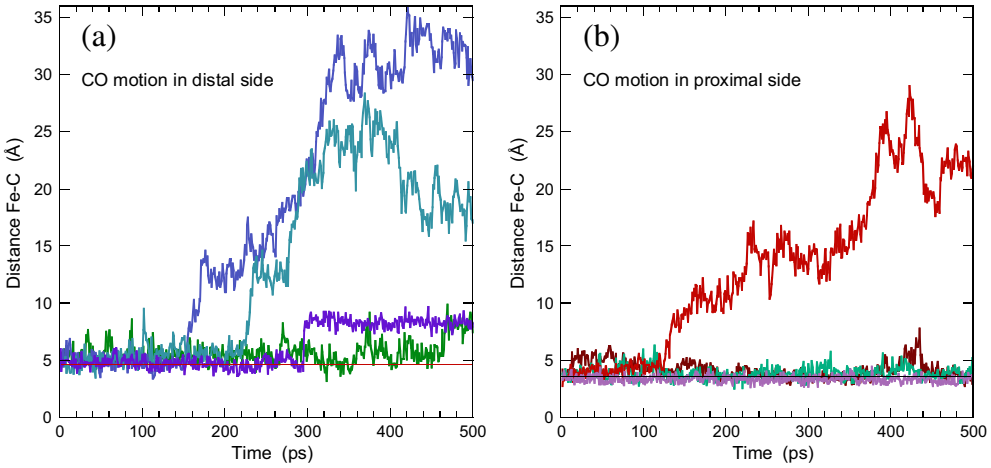

FIGURE 5 Distance between the Fe^{2+} and the carbon atom of CO during simulated dynamics of CO within the heme pocket of H93C Mb after CO dissociation in the distal (a) and the proximal side (b). "Proximal" and "distal" refer to coordination in WT Mb. The horizontal straight lines represent the mean closest position at 4.8 and 3.5 Å respectively.

TABLE 3 Comparison of the multi-exponential CO rebinding to H93C Mb with other heme proteins.

Protein	τ_1 (A_1)	τ_2 (A_2)	τ_3 (A_3)	Cst (A_0)	Reference
H93C Mb	12 ps (0.10)	248 ps (0.15)	1.8 ns (0.13)	0.62	This work
sGC	6.0 ps (0.07)	120 ps (0.01)	5.7 ns (0.05)	0.87	Yoo, Lamarre, Rappaport, et al. (2012)
sGC/BAY	6.0 ps (0.09)	90 ps (0.20)	1.2 ns (0.13)	0.58	Yoo, Lamarre, Rappaport, et al. (2012)
sGC-β_1(200)/BAY	10 ps (0.18)	100 ps (0.22)	800 ps (0.17)	0.43	Yoo, Lamarre, Rappaport, et al. (2012)
Cb H-NOX	7 (0.05)	100 ps (0.03)	8 ns (0.08)	0.84	Yoo, Lamarre, Rappaport, et al. (2012)
AXCP	–	218 ps (0.04)	1.9 ns (0.58)	0.38	Andrew et al. (2016)
L16A AXCP	–	543 ps (0.18)	3.6 ps (0.82)	0.00	Andrew et al. (2016)
CooA	78 ps (0.60)	390 ps (0.30)	–	0.10	Kumazaki et al. (2000)
DosH	–	–	1.5 ns (0.60)	0.40	Liebl et al. (2003)

Note: Time constants (τ_i) are given with their relative amplitudes A_i such that $\Sigma A_i = 1$. The constant A_0 represents the sum of all components with $\tau > 10$ ns and corresponds to bimolecular rebinding of CO from solution. BAY, sGC stimulator BAY 41-2272.

TABLE 4 Comparison of the multi-exponential NO rebinding to H93C Mb with other heme proteins.

Protein	Coordination	τ_1 (ps)	A_1	τ_2 (ps)	A_2	A_0	Ref
WT Mb	6c-(His)-NO	13	0.40	147	0.47	0.14	Kruglik et al. (2010)
H93C Mb	5c-NO	6.9	0.89	96[c]	0.09	0.02	This work
sGC	5c-NO	7.5	0.96	70[c]	0.02	0.02	Yoo, Lamarre, Martin, and Negrerie (2012)
AXCP[a]	5c-NO	7.0	0.98	100[c]	0.02	–	Yoo et al. (2013)
Cb H-NOX[b] at 20°C	5c-NO	7.1	0.87	–	–	<0.01	Yoo et al. (2023)
	6c-(His)-NO	–	–	24	0.13		

Note: Time constants (τ_i) and their relative amplitudes A_i such that $\Sigma A_i = 1$.
[a]*Alcaligenes xylosoxydans* cytchrome c′.
[b]H-NOX sensor from baterium *Clostridium botulinum*.
[c]Assigned to His rebinding.

Heme proteins which disclose a CO rebinding component in the ~80–500 ps range, like AXCP, the CO-sensor CooA (Kumazaki et al., 2000) or the O_2-sensor DOS (Liebl et al., 2003) form a 6c-(His)-CO species and rebind to the 5c-His heme. In the case of H93C Mb-CO the transient spectral components are identical to those observed in sGC in the presence of the stimulator BAY 41-2272 which is thus inferred to induce a 5c-CO heme. Cleavage of the Fe^{2+}–His bond by CO rationalizes its synergistic activation of sGC in the presence BAY 41-2272 (Yoo, Lamarre, Rappaport, et al., 2012).

Protein structures of H93C Mb and sGC are entirely different: sGC structure imposes a strain on its proximal histidine which gives rise to the weakening of the Fe^{2+}–His so that the NO *trans* effect, also observed in bacterial AXCP, leads to the 5c-NO species. The NO geminate

rebinding to the 4c heme always proceeds with a mono-exponential ~7-ps time constant (Table 4) (Kruglik et al., 2007; Negrerie et al., 2001; Yoo et al., 2015, 2023) which seems the limit value for this barrierless process. A second slower kinetic component can be present due to His rebinding to the 4c heme (Yoo et al., 2013, 2015) or to a minor form of 6c-(His)-NO (Yoo et al., 2023). In case of H93C Mb, the second component ($\tau_2 = 96$ ps) is due to His rebinding to the 4c heme. Many previous studies have shown that NO rebinds to various Mb mutants with bi-exponential kinetics (Brunori et al., 1999; Kholodenko et al., 1999; Petrich et al., 1994) but all are 6c-(His)-NO complex, contrarily to H93C Mb.

In summary, the single mutation His93Cys of the proximal histidine in Mb induces constraints due to the increase of Fe^{2+}–S distance so that the distal His64 can bind to the heme iron. In this case the negative *trans* effect due to NO induces the cleavage of the Fe^{2+}–His64 bond like in H-NOX sensors, whereas the strain on His64 ligation is sufficient to counteract the positive *trans* effect due to CO. In light of the similar CO dynamics in H93C Mb and activated sGC we can infer that the activator BAY 41-2272 induces further strain onto proximal His in sGC leading to a 5c-CO species.

3 | EXPERIMENTAL METHODS

3.1 | Preparation of H93C myoglobin mutant

The expression and purification of H93C Mb mutant were performed as previously described (Hildebrand et al., 1995). Briefly, the H93C mutation was introduced into the Mb gene and the DNA was transformed into competent *Escherichia coli* cells grown on agar plates. Isolated colonies were grown overnight at 37°C then isopropyl β-D-1-thiogalactopyranoside was added. After an additional 18-h growth the cells were centrifuged and resuspended in lysis buffer (50 mM NaH_2PO_4, 300 mM NaCl, 10 mM imidazole, 1 mg/mL lysozyme, pH 6). The expressed H93C Mb was collected by centrifugation and the supernatant concentrated. Further purification was performed on an ion exchange column with new buffer (100 mM KH_2PO_4, pH 7) and the protein was concentrated to ~100 μM.

3.2 | Preparation of samples for spectroscopy

The purified ferric protein was dissolved in phosphate buffer (pH 7.4) to ~30 μM and 100 μL of solution were put in a 1-mm optical pathlength quartz cell sealed with a rubber stopper and degassed by means of four successive cycles of vacuuming and purging with argon (Air Liquide, 99.999%). To obtain ferrous species, the ferric Mb was reduced by directly adding into the cell 10 μL of degased solution of sodium dithionite ($Na_2S_2O_4$) at 2 mM final concentration. For preparing NO-liganded protein, the argon gas phase (~300 μL) was replaced by 10% NO gas phase diluted in N_2, or 100% CO, directly introduced into the spectroscopic cell (final pressure ~ 1.3 bar). A second stopper in silicone with vacuum grease was placed over the first one to ensure gastightness.

3.3 | Picosecond time-resolved absorption spectroscopy

Transient spectra were recorded simultaneously to kinetics as a time-wavelength matrix data using the pump-probe laser system previously described (Negrerie, Cianetti, et al., 2006). Photodissociation of NO was achieved by excitation in the Q-bands of the heme ($\lambda_{ex} = 564$ nm; pulse duration ~50 fs; repetition rate 30 Hz). The entire transient absorption spectrum after a variable delay between dissociating and probe pulses was recorded with a cooled CCD detector. Equilibrium spectra were recorded with a Shimadzu 1700 spectrometer in the same cell. The accuracy for wavelength determination is ±0.5 nm for steady-state and ±1 nm for transient spectra. Measurements were performed at 20°C.

A reference pulse (same energy and spectrum as the probe pulse) is simultaneously recorded, allowing to calculate the absolute absorbance at each wavelength and time delay. Because photoexcitation is performed in non-saturating conditions to keep the response linear, there is a contribution from non photodissociated liganded heme which is removed when subtracting the spectrum before excitation from that at a given time delay.

3.4 | Analysis of the data

The global analysis of the data was performed by singular value decomposition (SVD) of the time-wavelength matrix (Negrerie, Cianetti, et al., 2006). Since we recorded a series of transient spectra at different time delays, the resulting data consists of a matrix of differential absorption as a function of time and wavelength $\Delta A(\lambda,t)$ which was decomposed according to:

$$\Delta A(\lambda,t) = \Delta A^{SVD}(\lambda) S K^{SVD}(t)$$

giving the orthogonal spectral component matrix $\Delta A^{SVD}(\lambda)$ and their associated kinetics matrix $K^{SVD}(t)$ weighted according to the singular values S_i (elements of

the diagonal matrix S). SVD kinetics represent the evolution of the associated differential spectra. The SDV spectra allowed to identify the underlining process. A SVD component may contain the contribution of several transitions due to large overlapping of the spectra of species.

The singular values of the two major SVD components are presented together with kinetics $K^{SVD}(t)$ and spectra $\Delta A^{SVD}(\lambda)$. Other SVD component of much lower singular values were negligible and not taken into account for further analysis. The individual kinetic components $K_j^{SVD}(t)$ were fitted to a multiexponential function:

$$f(t) = \sum\nolimits_i A_i \exp(-k_i t) + A_0$$

where the minimal number i of exponentials was determined iteratively. An asymptotic constant value (A_0) was included in some fits to account for time constants >10 ns. Alternatively, we performed a global analysis with the software Glotaran (Snellenburg et al., 2012) of the data matrix in the case of the CO complex, introducing the minimum number of exponential decays to obtain an ensemble of spectra associated with a unique time constant (DAS).

3.5 | Dynamics calculations of CO motion

We have built a model of whale MbCO H93C protein using the file 1A6G from the Protein Data Bank (Vojtechovsky et al., 1999) as a starting structure, replacing the proximal histidine with a cysteine. The structure is placed in a tetragonal water box with a unit cell dimension of about 80 Å. K^+ and Cl^- ions are added to cancel the total charge and simulate an ionic environment. The model includes of a polypeptide chain of 153 amino acids, one heme, one CO molecule, 16,108 water molecules, 24 Cl^- ions and 23 K^+ ions, comprising a total of 50,902 atoms. All molecular dynamics simulations are performed using CHARMM software (Brooks et al., 2009) with parameters version 36. A three-charge model is used to simulate the dipole and quadrupole moments of the CO molecule. Periodic boundary conditions have been assumed and the particle mesh Ewald method was used to compute efficiently all long range electrostatic interactions. After energy minimization, the temperature of the structure is gradually increased from 100 to 300 K for 100 ps, equilibrated at constant pressure for 250 ps, and finally at constant volume for 250 ps. After a free dynamic of 750 ps, the CO molecule is constrained to be inserted in the proximal or distal heme pocket using a harmonic potential for 250 ps. The constraints were released before a 500 ps free simulation and the distance of carbon atom to the iron atom was calculated each 1 ps. Two simulations of the CO motion inside proximal or distal heme pocket were performed with different initial conditions.

AUTHOR CONTRIBUTIONS

Byung-Kuk Yoo: Investigation; formal analysis; writing – original draft. **Jean-Christophe Lambry:** Investigation; writing – review and editing. **Michel Negrerie:** Conceptualization; investigation; writing – original draft; writing – review and editing; supervision.

ACKNOWLEDGMENTS

We thank Michael F. Davis for the gift of the Mb mutant.

ORCID

Michel Negrerie https://orcid.org/0000-0001-9918-031X

REFERENCES

Adachi S, Nagano S, Ishimori K, Watanabe Y, Morishima I, Egawa T, et al. Roles of proximal ligand in heme proteins: replacement of proximal histidine of human myoglobin with cysteine and tyrosine by site-directed mutagenesis as models for P-450, chloroperoxidase, and catalase. Biochemistry. 1993;32:241–52.

Adachi S, Nagano S, Watanabe Y, Ishimori K, Morishima I. Alteration of human myoglobin proximal histidine to cysteine or tyrosine by site-directed mutagenesis – characterization and their catalytic activities. Biochem Biophys Res Commun. 1991; 180:138–44.

Andrew CR, Petrova ON, Lamarre I, Lambry J-C, Rappaport F, Negrerie M. The dynamics behind the affinity: controling heme-gas affinity via geminate recombination and heme propionate conformation in the NO-carrier cytochrome c'. ACS Chem Biol. 2016;11:3191–201.

Barrick D. Replacement of the proximal ligand of sperm whale myoglobin with free imidazole in the mutant His93→Gly. Biochemistry. 1994;33:6546–54.

Brooks BR, MacKerell AD, Nilsson L, Petrella RJ, Roux B, Won Y, et al. CHARMM: the biomolecular simulation program. J Comput Chem. 2009;30:1545–614.

Brunori M, Cutruzzola F, Savino C, Travaglini-Allocatelli C, Vallone B, Gibson QH. Structural dynamics of ligand diffusion in the protein matrix: a study on a new myoglobin mutant Y(B10) Q(E7) R(E10). Biophys J. 1999;76:1259–69.

Cao W, Ye X, Sjodin T, Christian JF, Demidov AA, Berezhna S, et al. Investigations of photolysis and rebinding kinetics in myoglobin using proximal ligand replacements. Biochemistry. 2004;43:11109–17.

Crane BR, Arvai AS, Ghosh DK, Wu C, Getzoff ED, Stuehr DJ, et al. Structure of nitric oxide synthase oxygenase dimer with pterin and substrate. Science. 1998;279:2121–6.

Decatur SM, Franzen S, DePillis GD, Dyer RB, Woodruff WH, Boxer SG. Trans effects in nitric oxide binding to myoglobin cavity mutant H93G. Biochemistry. 1996;35:4939–44.

DePillis GD, Decatur SM, Barrick D, Boxer SG. Functional cavities in proteins: a general method for proximal ligand substitution in myoglobin. J Am Chem Soc. 1994;116:6981–2.

Dierks EA, Hu S, Vogel KM, Yu AE, Spiro TG, Burstyn JN. Demonstration of the role of scission of the proximal histidine-iron bond in the activation of soluble guanylyl cyclase through metalloporphyrin substitution studies. J Am Chem Soc. 1997; 119:7316–23.

Follmann M, Griebenow N, Hahn MG, Hartung I, Mais F-J, Mittendorf J, et al. The chemistry and biology of soluble guanylate cyclase stimulators and activators. Angew Chem Int Ed. 2013;52:1–23.

Franzen S. Spin-dependent mechanism for diatomic ligand binding to heme. Proc Natl Acad Sci U S A. 2002;99:16754–9.

Gautier C, Negrerie M, Wang Z-Q, Lambry J-C, Stuehr DJ, Collin F, et al. Dynamic regulation of the inducible nitric-oxide synthase by NO: comparaison with the endothelial isoform. J Biol Chem. 2004;279:4358–65.

Gullotti M, Santagostini L, Monzani E, Casella L. Effect of strain in the proximal ligand on the binding of nitric oxide and carbon monoxide to chelated protoheme complexes. Inorg Chem. 2007;46:8971–5.

Hildebrand DP, Ferrer JC, Tang HL, Smith M, Mauk AG. Trans effects on cysteine ligation in the proximal His93Cys variant of horse heart myoglobin. Biochemistry. 1995;34:11598–605.

Hoshino M, Maeda M, Konishi R, Seki H, Ford PC. Studies on the reaction mechanism for reductive nitrosylation of ferrihemoproteins in buffer solutions. J Am Chem Soc. 1996;118:5702–7.

Hoshino M, Ozawa K, Seki H, Ford PC. Photochemistry of nitric-oxide adducts of water-soluble iron(III) porphyrin and ferrihemoproteins studied by nanosecond laser photolysis. J Am Chem Soc. 1993;115:9568–75.

Hu X, Feng C, Hazzard JT, Tollin G, Montfort WR. Binding of YC-1 or BAY 41-2272 to soluble guanylyl cyclase induces a geminate phase in CO photolysis. J Am Chem Soc. 2008;130:15748–9.

Hunt AP, Lehnert N. Heme-nitrosyls: electronic structure implications for function in biology. Acc Chem Res. 2015;48:2117–25.

Ibrahim M, Kerby RL, Puranik M, Wasbotten IH, Youn H, Roberts GP, et al. Heme displacement mechanism of CooA activation: mutational and Raman spectroscopic evidence. J Biol Chem. 2006;281:29165–73.

Ionascu D, Gruia F, Ye X, Yu AC, Rosca F, Beck C, et al. Temperature-dependent studies of NO recombination to heme and heme proteins. J Am Chem Soc. 2005;127:16921–34.

Kang Y, Liu R, Wu J-X, Chen L. Structural insights into the mechanism of human soluble guanylate cyclase. Nature. 2019;574: 206–10.

Kholodenko Y, Gooding EA, Dou Y, Ikeda-Saito M, Hochstrasser RM. Heme protein dynamics revealed by geminate nitric oxide recombination in mutants of iron and cobalt myoglobin. Biochemistry. 1999;38:5918–24.

Kruglik SG, Lambry JC, Cianetti S, Martin J-L, Eady RR, Andrew CR, et al. Molecular basis for nitric oxide dynamics and affinity with *Alcaligenes xylosoxidans* cytochrome c'. J Biol Chem. 2007;282:5053–62.

Kruglik SG, Yoo B-K, Franzen S, Vos MH, Martin J-L, Negrerie M. Picosecond primary structural transition of the heme is retarded after nitric oxide binding to heme proteins. Proc Natl Acad Sci U S A. 2010;107:13678–783.

Kumazaki S, Nakajima H, Sakaguchi T, Nakagawa E, Shinohara H, Yoshihara K, et al. Dissociation and recombination between ligands and heme in a CO-sensing transcriptional activator CooA – a flash photolysis study. J Biol Chem. 2000;275: 38378–83.

Li Z, Pal B, Takenaka S, Tsuyama S, Kitagawa T. Resonance Raman evidence for the presence of two heme pocket conformations with varied activities in CO-bound bovine soluble guanylate cyclase and their conversion. Biochemistry. 2005; 44:939–46.

Liebl U, Bouzhir-Sima L, Kiger L, Marden MC, Lambry JC, Negrerie M, et al. Ligand binding dynamics to the heme domain of the oxygen sensor DOS from *Escherichia coli*. Biochemistry. 2003;42:6527–35.

Makino R, Obata Y, Tsubaki M, Iizuka T, Hamajima Y, Kato-Yamada Y, et al. Mechanistic insights into the activation of soluble guanylate cyclase by carbon monoxide: a multistep mechanism proposed for the BAY 41-2272 induced formation of 5-coordinate CO-heme. Biochemistry. 2018;57:1620–31.

Marti MA, Capece L, Crespo A, Doctorovich F, Estrin DA. Nitric oxide interaction with cytochrome c' and its relevance to guanylate cyclase. Why does the iron histidine bond break? J Am Chem Soc. 2005;127:7721–8.

Marti MA, Scherlis DA, Doctorovich FA, Ordejon P, Estrin DA. Modulation of the NO trans effect in heme proteins: implications for the activation of soluble guanylate cyclase. J Biol Inorg Chem. 2003;8:595–600.

Martin E, Czarnecki K, Jayaraman V, Murad F, Kincaid J. Resonance Raman and infrared spectroscopic studies of high-output forms of human soluble guanylyl cyclase. J Am Chem Soc. 2005;127:4625–31.

Matsui T, Nagano S, Ishimori K, Watanabe Y, Morishima I. Preparation and reactions of myoglobin mutants bearing both proximal cysteine ligand and hydrophobic distal cavity: protein models for the active site of P450. Biochemistry. 1996;35: 13118–24.

Messerschmidt A, Huber R, Wieghardt K, Cygler M, Poulos T, Bode W. Handbook of metalloproteins. Vol 1. Chichester: John Wiley; 2001. p. 1472.

Negrerie M. Iron transitions during activation of allosteric heme proteins in cell signaling. Metallomics. 2019;11:868–93.

Negrerie M, Berka V, Vos MH, Liebl U, Lambry J-C, Tsai A-L, et al. Geminate recombination of nitric oxide to endothelial nitric oxide-synthase and mechanistic implications. J Biol Chem. 1999;274:24694–702.

Negrerie M, Bouzhir L, Martin JL, Liebl U. Control of nitric oxide dynamics by guanylate cyclase in its activated state. J Biol Chem. 2001;276:46815–21.

Negrerie M, Cianetti S, Vos MH, Martin JL, Kruglik SG. Ultrafast heme dynamics in ferrous versus ferric cytochrome c studied by time-resolved resonance Raman and transient absorption spectroscopy. J Phys Chem B. 2006;110:12766–81.

Negrerie M, Kruglik SG, Lambry JC, Vos MH, Martin JL, Franzen S. Role of heme iron coordination and protein structure in the dynamics and geminate rebinding of nitric oxide to the H93G myoglobin mutant: implications for nitric oxide sensors. J Biol Chem. 2006;281:10389–98.

Petrich JW, Lambry JC, Balasubramanian S, Lambright DG, Boxer SG, Martin JL. Ultrafast measurements of geminate recombination of NO with site-specific mutants of human myoglobin. J Mol Biol. 1994;238:437–44.

Petruk AA, Vergara A, Estrin D, Merlino A. Molecular basis of the trans influence in quaternary T-state human hemoglobin: a computational study. FEBS Lett. 2013;587:2393–8.

Sage JT, Li P, Champion PM. Spectroscopic studies of myoglobin at low pH: heme ligation kinetics. Biochemistry. 1991;30:1237–47.

Schotte F, Lim MH, Jackson TA, Smirnov AV, Soman J, Olson JS, et al. Watching a protein as it functions with 150-ps time-resolved X-ray crystallography. Science. 2003;300:1944–7.

Shimizu T, Huang D, Yan F, Stranava M, Bartosova M, Fojtíková V, et al. Gaseous O_2, NO, and CO in signal transduction: structure and function relationships of heme-based gas sensors and heme-redox sensors. Chem Rev. 2015;115:6491–533.

Snellenburg JJ, Laptenok SP, Seger R, Mullen KM, van Stokkum IHM. Glotaran: a Java-based graphical user interface for the R package TIMP. J Stat Software. 2012;49:1–22.

Traylor TG, Sharma VS. Why NO? Biochemistry. 1992;31:2847–9.

Vojtechovsky J, Chu K, Berendzen J, Sweet RM, Schlichting I. Crystal structures of myoglobin-ligand complexes at near-atomic resolution. Biophys J. 1999;77:2153–74.

Wayland BB, Mehne LF, Swartz J. Mono- and biscarbonyl complexes of iron(II) tetraphenylporphyrin. J Am Chem Soc. 1978;100:2379–83.

Yoo B-K, Kruglik SG, Lambry J-C, Lamarre I, Raman CS, Nioche P, et al. The H-NOX protein structure adapts to different mechanisms in sensors interacting with nitric oxide. Chem Sci. 2023;14:8408–20.

Yoo B-K, Lamarre I, Martin J-L, Andrew CR, Negrerie M. Picosecond binding of the His ligand to four-coordinate heme in cytochrome c′: a one-way gate for releasing proximal NO. J Am Chem Soc. 2013;135:3248–54.

Yoo B-K, Lamarre I, Martin J-L, Negrerie M. Quaternary structure controls ligand dynamics in soluble guanylate cyclase. J Biol Chem. 2012;287:6851–9.

Yoo B-K, Lamarre I, Martin J-L, Rappaport F, Negrerie M. Motion of proximal histidine and structural allosteric transition in soluble guanylate cyclase. Proc Natl Acad Sci U S A. 2015;112:E1697–704.

Yoo BK, Lamarre I, Rappaport F, Nioche P, Raman CS, Martin JL, et al. Picosecond to second dynamics reveals a structural transition in *Clostridium botulinum* NO-sensor triggered by the activator BAY-41-2272. ACS Chem Biol. 2012;7:2046–54.

Yoshioka S, Takahashi S, Hori H, Ishimori K, Morishima I. Proximal cysteine residue is essential for the enzymatic activities of cytochrome P450(cam). Eur J Biochem. 2001;268:252–9.

Yu AE, Hu S, Spiro TG, Burstyn JN. Resonance Raman spectroscopy of soluble guanylate cyclase reveals displacement of distal and proximal heme ligands by NO. J Am Chem Soc. 1994;116:4117–8.

Zhao Y, Brandish PE, Ballou DP, Marletta MA. A molecular basis for nitric oxide sensing by soluble guanylate cyclase. Proc Natl Acad Sci U S A. 1999;96:14753–8.

How to cite this article: Yoo B-K, Lambry J-C, Negrerie M. Controlling the *trans* effect induced by nitric oxide and carbon monoxide: H93C myoglobin versus H-NOX sensors and soluble guanylate cyclase. Protein Science. 2024;33(12):e5231. https://doi.org/10.1002/pro.5231